Giant magnetocaloric effect in melt-spun Ni-Mn-Ga ribbons with magneto-multistructural transformation

Zongbin Li, Yudong Zhang, C. F. Sánchez-Valdés, J. L. Sánchez Llamazares, Claude Esling, Xiang Zhao, and Liang Zuo

Citation: Appl. Phys. Lett. **104**, 044101 (2014);
View online: https://doi.org/10.1063/1.4863273
View Table of Contents: http://aip.scitation.org/toc/apl/104/4
Published by the American Institute of Physics

Giant magnetocaloric effect in melt-spun Ni-Mn-Ga ribbons with magneto-multistructural transformation

Zongbin Li,[1] Yudong Zhang,[2,3] C. F. Sánchez-Valdés,[4] J. L. Sánchez Llamazares,[4] Claude Esling,[2,3] Xiang Zhao,[1] and Liang Zuo[1,a)]

[1]*Key Laboratory for Anisotropy and Texture of Materials (Ministry of Education), Northeastern University, Shenyang 110819, China*

[2]*Laboratoire d'Étude des Microstructures et de Mécanique des Matériaux (LEM3), CNRS UMR 7239, Université de Lorraine, 57045 Metz, France*

[3]*Laboratory of Excellence on Design of Alloy Metals for low-mAss Structures (DAMAS), Université de Lorraine, 57045 Metz, France*

[4]*Instituto Potosino de Investigación Científica y Tecnológica A.C., Camino a la Presa San José 2055, Col. Lomas 4ª, San Luis Potosí, S.L.P. 78216, Mexico*

(Received 23 November 2013; accepted 7 January 2014; published online 27 January 2014)

Magnetic refrigeration based on the magnetocaloric effect (MCE) may provide an energy-efficient and environment-friendly alternative to the conventional gas compression/expansion cooling technology. For potential applications, low-cost and high-performance magnetic refrigerants are in great need. Here, we demonstrate that giant MCE can be achieved in annealed $Ni_{52}Mn_{26}Ga_{22}$ ribbons with magneto-multistructural transformation. It yields a maximum magnetic entropy change of $-30.0\ J\ kg^{-1}\ K^{-1}$ at the magnetic field change of 5 T, being almost three times as that of initial melt-spun ribbons and comparable to or even superior to that of polycrystalline bulk alloys. [http://dx.doi.org/10.1063/1.4863273]

The magnetocaloric effect (MCE) is an intrinsic magneto-thermodynamic property of magnetic materials, quantified by magnetic entropy change ΔS_M or adiabatic temperature change ΔT_{ad} when subjected to a magnetic field change $\mu_o \Delta H$.[1] Based on this effect, magnetic refrigeration has been demonstrated to be an energy-efficient and environment-friendly alternative to conventional vapor-cycle refrigeration technology. In search for prospective magnetic refrigerant materials, ferromagnetic Ni-Mn-X (X = Ga, In, Sn, and Sb) Heusler-type alloys[2–8] are of particular interest. Such alloys exhibit thermoelastic martensitic transformation with a wide tunable temperature range, and the combined structural and magnetic contributions bring about not only considerable magnetic shape memory effect[9–11] but also giant MCE.[2,3,5,7,8]

For Ni-Mn-Ga alloys, a large entropy change can be induced by magnetic field change at the vicinity of martensitic or magnetic transition.[12] If the martensitic transformation is tuned to be coupled with the magnetic transition, i.e., the magnetostructural transformation, the MCE becomes giant.[3,12] Currently, large MCE has been observed in single crystals,[3] polycrystalline bulk alloys,[12–20] and melt-spun ribbons[21,22] with magneto-unistructural transformation. The highest ΔS_M of $-86\ J\ kg^{-1}\ K^{-1}$ was achieved in single-crystalline $Ni_{55}Mn_{20}Ga_{25}$ alloy at a magnetic field change of about 5 T.[3] However, the high cost and complexity associated with the fabrication of single crystals becomes an unavoidable hindrance for practical applications.

Magnetic refrigerant materials are more likely to be used in polycrystalline form, since they can be produced at relatively low cost and on large scale using continuous fabrication processes such as casting, melt-spinning, and sintering. Obviously, the existence of crystal defects in polycrystalline alloys would lower the magnetic entropy change and hence the MCE. For example, the ΔS_M was found to be $-20.4\ J\ kg^{-1}\ K^{-1}$ in polycrystalline $Ni_{55.2}Mn_{18.6}Ga_{26.2}$ bulk alloy[13] and $-20\ J\ kg^{-1}\ K^{-1}$ in polycrystalline $Ni_{57.25}Mn_{22.25}Ga_{20.5}$ bulk alloy[17] under $\mu_o \Delta H = 5$ T.

In general, bulk Heusler-type alloys are intrinsically brittle and thus difficult to be processed. As a viable alternative to conventional preparation, the rapid solidification by melt-spinning has proven to be an effective single-step route for fabricating refrigerant alloys.[4,6,21–25] This approach can lower the brittleness of produced materials through microstructure refinement. Moreover, it may offer an ideal geometrical shape for use in refrigeration devices, as the influence of the demagnetizing factor on the ΔS_M becomes negligible when ribbon-shaped refrigerants are magnetized along their longitudinal directions. Therefore, thin ribbons produced by melt-spinning seem to be more promising for practical applications in view of their mechanical properties and the demagnetization effect. However, the enhanced atomic disordering in fine-grained ribbons may lead to a much decreased ΔS_M, even less than that of polycrystalline bulk alloys. Our recent work has shown that the maximum ΔS_M in melt-spun $Ni_{52}Mn_{26}Ga_{22}$ ribbons with magnetostructural transformation is $-11.4\ J\ kg^{-1}\ K^{-1}$ under $\mu_o \Delta H = 5$ T.[22]

From the survey of the literature, one can find that the state of atomic ordering and the occurrence of magnetostructural transformation are the key factors that influence the ΔS_M of Ni-Mn-Ga alloys. On one hand, the existence of grain boundaries in polycrystalline alloys decreases the ΔS_M. On the other hand, a simultaneous magnetic and structure transformation maximizes the ΔS_M. It should be noted that two types of structural transformations, namely, martensitic transformation and intermartensitic transformation,[26–28] have been evidenced in Ni-Mn-Ga alloys upon cooling and

a)Author to whom correspondence should be addressed. Electronic mail: lzuo@mail.neu.edu.cn

heating. However, the second structural transformation remains to be explored for enhancing ΔS_M, as the simultaneity of the two structural transformations and the magnetic transition has not been reported in any previous work.

In this study, based on composition tuning, polycrystalline $Ni_{52}Mn_{26}Ga_{22}$ thin ribbons were prepared by melt-spinning.[22] The as-melt-spun ribbon samples were annealed in vacuum at 1173 K for 18 h, capable of enhancing the atomic ordering and introducing an intermartensitic transformation coupled with the magnetostructural transformation (i.e., the magneto-multistructural transformation). The characteristic martensitic transformation temperatures were measured by differential scanning calorimetry (DSC). The crystal structure was determined at room temperature by X-ray diffraction (XRD). The microstructural characterizations were performed in a field emission scanning electron microscope (SEM) with electron backscatter diffraction (EBSD). Magnetization measurements were performed by vibrating sample magnetometry in a Quantum Design PPMS® EverCool®-9T platform, where the magnetic field was applied along the longitudinal direction of the ribbon samples in order to minimize the effect of the internal demagnetizing field.

Fig. 1(a) shows the room temperature XRD patterns of the as-melt-spun and annealed $Ni_{52}Mn_{26}Ga_{22}$ ribbons. The

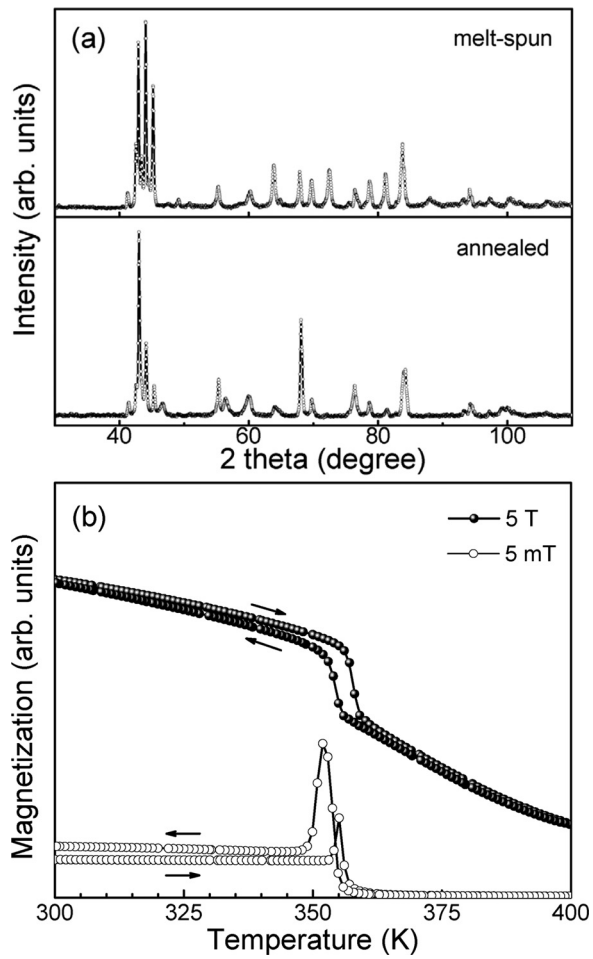

FIG. 1. (a) Room temperature XRD patterns of as-melt-spun (top) and annealed (bottom) ribbons. (b) Temperature-dependent magnetization $M(T)$ curves of annealed ribbons under magnetic field of 5 mT and 5 T. The arrows indicate the field-cooling and field-heating pathways.

as-melt-spun ribbons have a single-phase microstructure containing only seven-layered modulated (7M) martensite. In contrast, the annealed ribbons possess a mixture of 7M martensite and non-modulated (NM) martensite, suggesting the occurrence of the 7M to NM intermartensitic transformation induced by post-annealing. By Rietveld refinement analysis, the 7M martensite was determined to be a monoclinic incommensurate superstructure[28–30] with lattice constants $a = 4.263$ Å, $b = 5.523$ Å, $c = 42.265$ Å, and $\beta = 93.2°$, and the NM martensite a tetragonal structure with lattice constants $a = b = 3.882$ Å and $c = 6.531$ Å.

Table I presents the martensitic transformation temperatures (M_s, M_f, A_s, and A_f), and the magnetic transition temperature (T_C) of the as-melt-spun and annealed ribbons. For the annealed ribbons, certain increases are evident in the martensitic and magnetic transition temperatures due to the reduction of crystal defects. Moreover, from the temperature-dependent magnetization $M(T)$ curves [Fig. 1(b)], it is noted that the magnetic transition and the martensitic transformation occurred almost simultaneously. Together with the XRD phase identification, one can find that the magnetic transition is coupled with a two-step structural transition (austenite–7M–NM), i.e., magneto-multistructural transformation. Such a coupling has certainty not been reported for Ni-Mn-Ga alloys. As the austenite and martensite phases are, respectively, paramagnetic and ferromagnetic, an abrupt and relatively large magnetization change across the martensitic transformation is observed. By comparing the low-field (5 mT) and high-field (5 T) $M(T)$ curves [Fig. 1(b)], it is found that the application of a magnetic field of 5 T leads to an insignificant increase of the structural transformation temperatures (~3 K) at which the martensitic and intermartensitic transformations take place concurrently.

Fig. 2(a) shows the secondary electron image taken from the fractured cross-section of an annealed ribbon, where initial austenite grains are columnar in shape and stretch through the whole ribbon thickness. As compared to the as-melt-spun ribbons, the high temperature annealing has brought about a remarkable increase in the grain size of initial austenite, thus greatly reducing the amount of grain boundaries. Fig. 2(b) displays a typical backscattered electron (BSE) image taken from the ribbon plane of the annealed ribbon. The martensite plates that transformed from parent austenite grains (about 50–100 μm in size) are clustered in colonies. Further EBSD microstructural characterization has revealed that there exist both 7M and NM martensite in some original austenite grains. Figs. 2(c) and 2(d) present an EBSD phase-indexed map covering the co-existing 7M and NM martensite in one original austenite grain and the corresponding orientation map. Notably, the NM martensite plates are much thicker than the 7M martensite plates. As demonstrated previously,[28] the plate

TABLE I. Martensitic and magnetic transition temperatures of as-melt-spun and annealed ribbons determined from DSC and low-field $M(T)$ curves.

					T_C (K)	
Sample	M_S (K)	M_f (K)	A_S (K)	A_f (K)	Cooling	Heating
As-melt-spun	346	332	341	354	350	351
Annealed	353	339	348	361	354	356

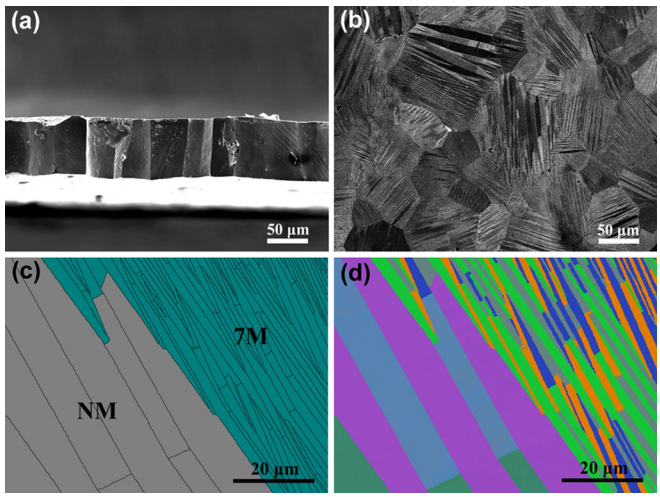

FIG. 2. (a) Secondary electron image from fractured cross-section of an annealed ribbon sample. (b) BSE image of the ribbon plane. (c) EBSD phase-indexed map showing the co-existence of 7M martensite and NM martensite in an original austenite grain, where 7M martensite is colored in green and NM martensite in grey. (d) EBSD orientation imaging map corresponding to Fig. 2(c).

interfaces of 7M martensite are coherent and should have low energy, whereas the plate interfaces of NM martensite are non-coherent with high energy. Thus, the intermartensitic transformation from 7M martensite to NM martensite is accompanied by plate thickening, which results in a reduction of the total interfacial energy. Moreover, it is found that the 7M to NM transformation always occurs in austenite grains with much larger size. This might be due to the fact that larger austenite grains are subject to less constraint from surroundings and have a propensity for 7M martensite to be further transformed into NM martensite.

Fig. 3(a) presents the magnetization isotherms $M(\mu_o H)$ of the annealed ribbons, measured up to a maximum applied field of $\mu_o H_{max} = 5\,\mathrm{T}$. As compared to the as-melt-spun ribbons, the martensite of the annealed ribbons possesses higher saturation magnetization (e.g., increased by 9.3% at 300 K). Using the measured $M(\mu_o H)$ curves, the isothermal magnetic entropy changes were calculated by numerical integration of the Maxwell relation,[31] i.e., $\Delta S_M(T) = \int_o^{B\max} (\partial M/\partial T)_B dB$. Fig. 3(b) plots the calculated ΔS_M values as a function of temperature under the field change of 2 T and 5 T. Notably, the ΔS_M reaches the maximum level (ΔS_M^{max}) at around 354 K, i.e., at the vicinity of the magneto-multistructural transition temperature. They are, respectively, $-16.4\ \mathrm{J\,kg^{-1}\,K^{-1}}$ and $-30.0\ \mathrm{J\,kg^{-1}\,K^{-1}}$ for $\mu_o \Delta H = 2\,\mathrm{T}$ and 5 T, being almost three times as those of the as-melt-spun ribbons (i.e., $-5.3\ \mathrm{J\,kg^{-1}\,K^{-1}}$ and $-11.4\ \mathrm{J\,kg^{-1}\,K^{-1}}$).[22] Besides, the observed ΔS_M^{max} values are also much higher than those reported for $Ni_{55}Mn_{20.6}Ga_{24.4}$ and $Ni_{55}Mn_{19.6}Ga_{25.4}$ ribbons (i.e., $-9.5\ \mathrm{J\,kg^{-1}\,K^{-1}}$ and $-10.4\ \mathrm{J\,kg^{-1}\,K^{-1}}$ at 309 K under $\mu_o \Delta H = 2\,\mathrm{T}$).[21] Such a remarkable increase of ΔS_M^{max} should be attributed to the enhanced atomic ordering and the magneto-multistructural coupling.

Fig. 4 presents the absolute ΔS_M^{max} values as a function of magnetic field change for the present annealed ribbons with magneto-multistructural transformation. They are comparable to or even higher than those reported for polycrystalline Ni-Mn-Ga bulk alloys having magneto-unistructural

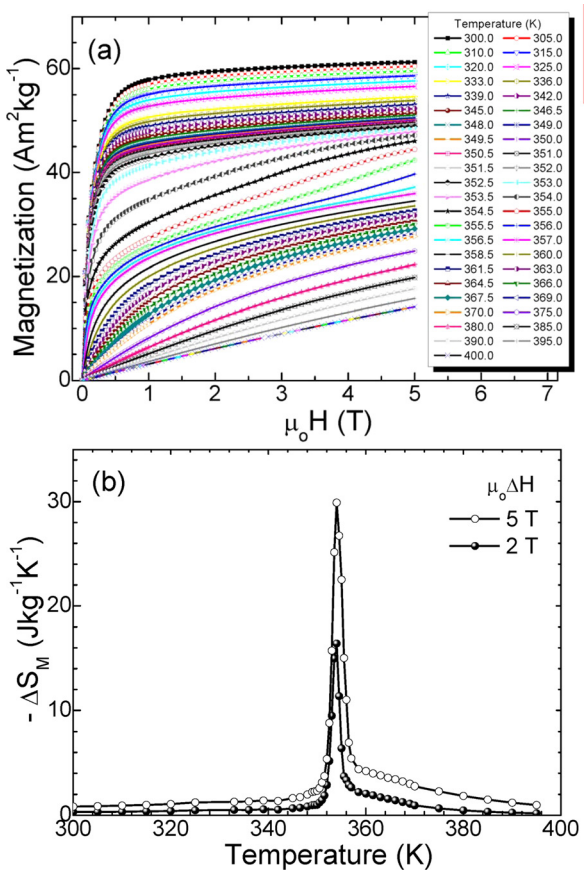

FIG. 3. (a) Isothermal magnetization curves $M(\mu_o H)$ in the temperature range of 300–400 K. (b) Temperature dependence of $-\Delta S_M$ under $\mu_o \Delta H = 2\,\mathrm{T}$ and 5 T. The thermomagnetic protocol followed to measure the isothermal magnetization curves has been carefully chosen in order to avoid any over- or under-estimation of $-\Delta S_M$ using the Maxwell relation. Note that the coincidence between the temperature at which maximum magnetic entropy change is attained and the temperature indicated by DSC and low-field $M(T)$ curves.

transformation. Moreover, to assess the usefulness of a magnetocaloric material, one should consider not only the magnitude of ΔS_M but also its temperature dependence. Here, the so-called refrigerant capacity (RC) is used to estimate the amount of thermal energy that can be transferred by

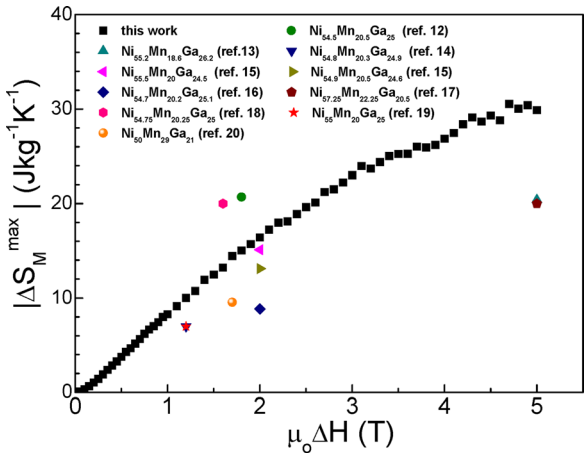

FIG. 4. Field dependence of maximum absolute magnetic entropy change—a comparison between the present annealed $Ni_{52}Mn_{26}Ga_{22}$ ribbons and the polycrystalline Ni-Mn-Ga bulk alloys reported in literature.

magnetic refrigerant between the cold and hot sinks in one ideal thermodynamic cycle.[32,33] In approximation, the *RC* is described by $RC = \Delta S_M^{max} \cdot \delta T_{FWHM}$, where δT_{FWHM} is the full width at half maximum (*FWHM*) of the $\Delta S_M(T)$ peak. For the present annealed ribbons, the *RC* values were calculated to be 75 J kg^{-1} ($\mu_o \Delta H = 5$ T) and 33 J kg^{-1} ($\mu_o \Delta H = 2$ T).

Fig. 5(a) and the inset of Fig. 5(b) show the field-up and field-down isothermal magnetization $M(\mu_o H)$ curves recorded, respectively, up to $\mu_o H_{max} = 5$ T and 2 T, where the inverse martensitic transformation was thermally induced. At the temperature range of 353–356 K, the demagnetization process exhibits magnetic hysteresis. The hysteresis loss values at different temperatures were determined by calculating the areas enclosed by the field-up and field-down $M(\mu_o H)$ curves.[23,32] Fig. 5(b) plots the hysteretic losses as a function of temperature for a field change of 2 T and 5 T, where the maximum loss reaches ~1.7 J kg^{-1} and ~11.3 J kg^{-1} at ~354.5 K. Note that the hysteretic losses reduce considerably for 2 T—a reference magnetic field change of practical importance for application. Certainly, the hysteretic losses associated with magnetic transition are detrimental to the *RC*.[32,33] By subtracting the average hysteretic losses, the effective *RC* values of the annealed ribbons were determined to be 70 J kg^{-1} and 32 J kg^{-1} for $\mu_o \Delta H_{max} = 5$ T and 2 T, respectively. Hence, the refrigerant capacity at 2 T is not significantly affected by the magnetic hysteretic loss.

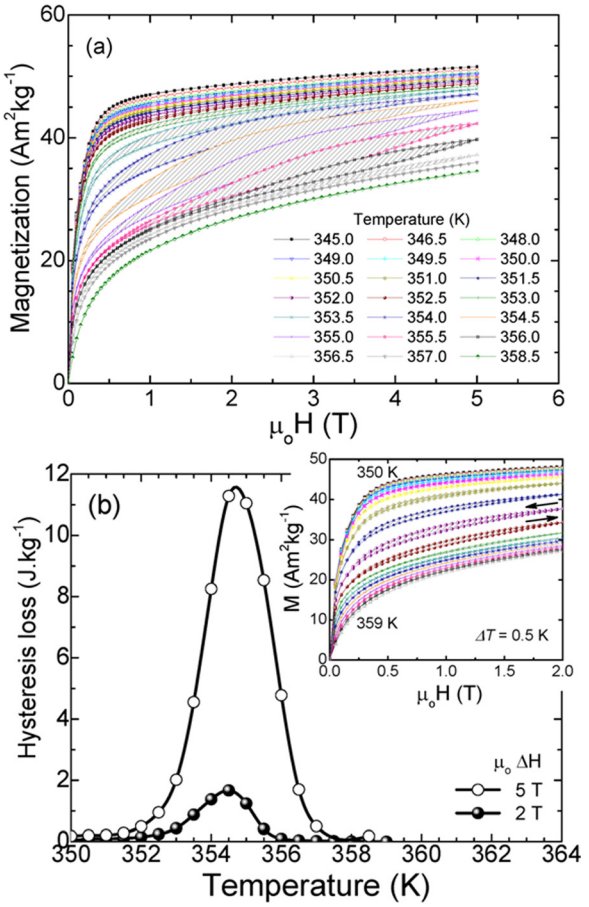

FIG. 5. (a) Field-up and field-down isothermal magnetization curves up to $\mu_o H_{max} = 5$ T. (b) Hysteresis losses as a function of temperature for $\mu_o \Delta H = 2$ T and 5 T across the martensite-to-austenite transformation. Inset: field-up and field-down isothermal magnetization curves up to $\mu_o H_{max} = 2$ T.

It is worth mentioning that the temperature range (353–356 K) exhibiting magnetic hysteresis in the annealed ribbons is just located within the temperature range of the magneto-multistructural transformation. From the slope change shown in the field-up and field-down $M(\mu_o H)$ curves [Fig. 5(a)], it is inferred that the transformation from paramagnetic austenite to ferromagnetic martensite was induced by magnetic field. Thus, the observed hysteresis should be originated from the field-induced phase transformation. As demonstrated in the present case, during the magneto-multistructural transformation, the structural transformation is no longer a single martensitic transformation from austenite to 7M martensite, but integrated with consecutive 7M to NM intermartensitic transformation. The occurrence of the intermartensitic transformation imposes an additional transformation barrier on the reversible magnetostructural transformation due to the crystal lattice distortion between the two martensitic phases and the interfacial energy change of their plate interfaces. In comparison with the forward two-step transformation, the inverse transformation from the ground state NM martensite to the austenite needs much larger driving force, which results in hysteresis loss under an applied magnetic field.

It should be emphasized that the maximum hysteresis losses observed in the annealed $Ni_{52}Mn_{26}Ga_{22}$ ribbons are close to those of polycrystalline Ni-Mn-Ga bulk alloys (i.e., ~12 J kg^{-1} at $\mu_o \Delta H = 5$ T),[34] but far below to the values reported for Ni-Mn-X (X = In, Sn, Sb) based alloys.[4,23,35–38] For example, a typical hysteresis loss of 95 J kg^{-1} was achieved in polycrystalline $Ni_{50}Mn_{34.95}In_{15.05}$ alloy at $\mu_o \Delta H = 5$ T.[35] In this context, polycrystalline Ni-Mn-Ga alloys with relatively low hysteresis loss could be more effective for magnetic refrigeration. Moreover, the same sign of enthalpy changes for the magnetic and structural transitions in Ni-Mn-Ga alloys avoids the impairment of the MCE due to the opposite heat processes,[8,39] which is different from the case of the ferromagnetic-antiferromagnetic/paramagnetic transitions in Ni-Mn-X (X = In, Sn, Sb) alloys.[4,23,35–38]

In summary, the magnetostructural transformation and the MCE of the melt-spun $Ni_{52}Mn_{26}Ga_{22}$ ribbons were studied. The annealing procedure renders strong coupling between the magnetic transition and the martensitic and intermartensitic transformations. The maximum ΔS_M of −30.0 J kg^{-1} K^{-1} is achieved under $\mu_o \Delta H = 5$ T, which represents the highest record for Ni-Mn-Ga ribbons, and it is comparable to or even higher than those of polycrystalline bulk alloys. The hysteresis loss level of the annealed ribbons is close to that in polycrystalline bulk alloys and in practice negligible for $\mu_o \Delta H = 2$ T. Thus, the fabrication of Ni-Mn-Ga alloys by proper composition tuning and melt-spinning with post-annealing could be an economical processing route to improve magnetocaloric properties.

This work was supported by the 863 Program of China (Grant No. 2014AAQ00297), the 111 Program of China (Grant No. B07015), the Program for Liaoning Innovative Research Team in University (Grant No. LT2013007), the joint French-Chinese Project (Grant No. ANR-09-BLAN-0382), and Sino-French Cai Yuanpei Program (Grant No. 24013QG). J. L. Sánchez Llamazares acknowledges the support from Laboratorio Nacional de Investigaciones en Nanociencias y

Nanotecnología (LINAN, IPICyT) and CONACYT, Mexico (Grant Nos. 156932 and 157541). C. F. Sánchez-Valdés thanks LINAN and IPICyT for supporting his postdoctoral stay.

[1]V. K. Pecharsky and K. A. Gschneidner, Jr., J. Magn. Magn. Mater. **200**, 44 (1999).
[2]A. Planes, L. Mañosa, and A. Acet, J. Phys.: Condens. Matter **21**, 233201 (2009).
[3]M. Pasquale, C. P. Sasso, L. H. Lewis, L. Giudici, T. Lograsso, and D. Schlagel, Phys. Rev. B **72**, 094435 (2005).
[4]B. Hernando, J. L. Sánchez Llamazares, J. D. Santos, V. M. Prida, D. Baldomir, D. Serantes, R. Varga, and J. González, Appl. Phys. Lett. **92**, 132507 (2008).
[5]M. Khan, N. Ali, and S. Stadler, J. Appl. Phys. **101**, 053919 (2007).
[6]J. L. Sánchez Llamazares, B. Hernando, C. García, J. González, L. Escoda, and J. J. Suñol, J. Phys. D: Appl. Phys. **42**, 045002 (2009).
[7]T. Krenke, E. Duman, M. Acet, E. F. Wassermann, X. Moya, L. Manosa, and A. Planes, Nature Mater. **4**, 450 (2005).
[8]J. Liu, T. Gottschall, K. P. Skokov, J. D. Moore, and O. Gutfleisch, Nature Mater. **11**, 620 (2012).
[9]S. J. Murray, M. Marioni, S. M. Allen, R. C. O'Handley, and T. A. Lograsso, Appl. Phys. Lett. **77**, 886 (2000).
[10]A. Sozinov, A. A. Likhachev, N. Lanska, and K. Ullakko, Appl. Phys. Lett. **80**, 1746 (2002).
[11]R. Kainuma, Y. Imano, W. Ito, Y. Sutou, H. Morito, S. Okamoto, O. Kitakami, K. Oikawa, A. Fujita, T. Kanomata, and K. Ishida, Nature **439**, 957 (2006).
[12]A. A. Cherechukin, T. Takagi, M. Matsumoto, and V. D. Buchel'nikov, Phys. Lett. A **326**, 146 (2004).
[13]X. Z. Zhou, W. Li, H. P. Kunkel, and G. Williams, J. Phys.: Condens. Matter **16**, L39 (2004).
[14]B. Ingale, R. Gopalan, M. Manivel Raja, V. Chandrasekaran, and S. Ram, J. Appl. Phys. **102**, 013906 (2007).
[15]Y. Long, Z. Y. Zhang, D. Wen, G. H. Wu, R. C. Ye, Y. Q. Chang, and F. R. Wan, J. Appl. Phys. **98**, 046102 (2005).
[16]J. F. Duan, P. Huang, H. Zhang, Y. Long, G. H. Wu, R. C. Ye, Y. Q. Chang, and F. R. Wan, J. Alloys Compd. **441**, 29 (2007).
[17]S. K. Srivastava, V. K. Srivastava, and R. Chatterjee, Solid State Commun. **152**, 372 (2012).
[18]L. Pareti, M. Solzi, F. Albertini, and A. Paoluzi, Eur. Phys. J. B **32**, 303 (2003).
[19]I. Babita, R. Gopalan, and S. Ram, J. Phys.: Conf. Ser. **144**, 012066 (2009).
[20]X. Zhou, H. Kunkel, G. Williams, S. Zhang, and D. Xue, J. Magn. Magn. Mater. **305**, 372 (2006).
[21]N. V. Rama Rao, R. Gopalan, V. Chandrasekaran, and K. G. Suresh, J. Alloys Compd. **478**, 59 (2009).
[22]Z. B. Li, J. L. Sánchez Llamazares, C. F. Sánchez-Valdés, Y. D. Zhang, C. Esling, X. Zhao, and L. Zuo, Appl. Phys. Lett. **100**, 174102 (2012).
[23]B. Hernando, J. L. Sánchez Llamazares, V. M. Prida, D. Baldomir, D. Serantes, M. Ilyn, and J. González, Appl. Phys. Lett. **94**, 222502 (2009).
[24]N. V. Rama Rao, R. Gopalan, M. Manivel Raja, J. Arout Chelvane, B. Majumdar, and V. Chandrasekaran, Scr. Mater. **56**, 405 (2007).
[25]J. Liu, T. G. Woodcock, N. Scheerbaum, and O. Gutfleisch, Acta Mater. **57**, 4911 (2009).
[26]C. Seguí, V. A. Chernenko, J. Pons, E. Cesari, V. Khovailo, and T. Takagi, Acta Mater. **53**, 111 (2005).
[27]W. H. Wang, Z. H. Liu, J. Zhang, J. L. Chen, G. H. Wu, W. S. Zhan, T. S. Chin, G. H. Wen, and X. X. Zhang, Phys. Rev. B **66**, 052411 (2002).
[28]Z. B. Li, Y. D. Zhang, C. Esling, X. Zhao, and L. Zuo, Acta Mater. **61**, 3858 (2013).
[29]Z. B. Li, Y. D. Zhang, C. Esling, X. Zhao, Y. D. Wang, and L. Zuo, J. Appl. Cryst. **43**, 617 (2010).
[30]L. Righi, F. Albertini, E. Villa, A. Paoluzi, G. Calestani, V. Chernenko, S. Besseghini, C. Ritter, and F. Passaretti, Acta Mater. **56**, 4529 (2008).
[31]A. M. Tishin and Y. I. Spichkin, *The Magnetocaloric Effect and Its Applications* (Institute of Physics Publishing, Bristol, 2003).
[32]N. S. Bingham, M. H. Phan, H. Srikanth, M. A. Torija, and C. Leighton, J. Appl. Phys. **106**, 023909 (2009).
[33]T.-L. Phan, P. Zhang, N. H. Dan, N. H. Yen, P. T. Thanh, T. D. Thanh, M. H. Phan, and S. C. Yu, Appl. Phys. Lett. **101**, 212403 (2012).
[34]S. Stadler, M. Khan, J. Mitchell, N. Ali, A. M. Gomes, I. Dubenko, A. Y. Takeuchi, and A. P. Guimarães, Appl. Phys. Lett. **88**, 192511 (2006).
[35]A. K. Pathak, M. Khan, I. Dubenko, S. Stadler, and N. Ali, Appl. Phys. Lett. **90**, 262504 (2007).
[36]P. J. Shamberger and F. S. Ohuchi, Phys. Rev. B. **79**, 144407 (2009).
[37]D. Bourgault, J. Tillier, P. Courtois, D. Maillard, and X. Chaud, Appl. Phys. Lett. **96**, 132501 (2010).
[38]A. K. Nayaka, N. V. Rama Raoa, K. G. Suresha, and A. K. Nigam, J. Alloys Compd. **499**, 140 (2010).
[39]E. K. Liu, W. H. Wang, L. Feng, W. Zhu, G. J. Li, J. L. Chen, H. W. Zhang, G. H. Wu, C. B. Jiang, H. B. Xu, and F. de Boer, Nat. Commun. **3**, 873 (2012).